A Simple and Accurate Matrix for Model Based Photoacoustic Imaging

K.J. Francis, Pradeep Mishra,
P. Rajalakshmi, Sumohana S. Channappayya
Dept. of Electrical Engineering,
Indian Institute of Technology Hyderabad
Hyderabad, India - 502285
Email: ee14resch12001@iith.ac.in,pradeepmishra@iith.ac.in
raji@iith.ac.in, sumohana@iith.ac.in

Ashutosh Richhariya
Institute of Translational Research
L V Prasad Eye Institute (LVPEI)
Hyderabad, India 500034
Email: ashutosh@lvpei.org

***Abstract*—Accurate model-based methods in Photo-Acoustic Tomography (PAT) can reconstruct the image from insufficient and inaccurate measurements. Most of the models either make the simplified assumption of spherical averaging or use accurate models that have computationally burdensome implementations. We present a simple and accurate measurement matrix that is derived from the pseudo-spectral PAT model. The accuracy of the measurement matrix is first validated against the experimental PAT signal. We also compare the model against the standard k-wave measurement model and the spherical averaging model. We then highlight several reconstruction strategies based on the nature of the region of interest to further demonstrate the accuracy of the proposed measurement matrix.**

I. Introduction

Photo-Acoustic Tomography (PAT) works on the principle of photoacoustic effect, in which optical absorbers convert energy from a pulsed laser to acoustic energy [1]. Using a light source preserves the contrast while the negligible scattering effect of ultrasound waves helps preserve resolution. The ability to probe endogenous contrast agents like oxyhemoglobin, deoxyhemoglobin, water, melanin and exogenous contrast agents like organic dye, nano-particles, has attracted many medical imaging applications in the last decade. Brain functional imaging, angiogenesis, drug response , gene activity, cancer detection are a few from the large number of applications reported [2]. Image reconstruction from the acoustic wave is performed mainly using analytical methods like back projection and time reversal. Even though computationally efficient, they are limited to specific geometries and require accurate and fairly large measurements. However, a majority of the PAT systems suffer from insufficient and noisy measurement. Though computationally expensive, model-based reconstruction methods can address this problem. These methods model the wave propagation in tissue as a linear system and inverting the model to reconstruct the image. Model-based methods can also incorporate arbitrary geometry, heterogeneity in medium and transducer properties. Measurement matrices in both the time [3] and frequency domains [4] have been proposed based on the Green's function solution to the standard PAT imaging model. These measurement matrices have been successfully used for l_1 or sparse signal recovery. Prakash et al. [5] considered a transducer impulse response based measurement matrix and studied signal reconstruction based on a least squares approach. All these matrices are based on the spherical averaging of the PAT wavefront. A matrix including inhomogeneous property of medium, absorption and dispersion with frequency is presented in [6] which is accurate but computationally intensive. We present a simple and accurate matrix that models wave propagation, starting from the pseudo-spectral solution for the PAT wave equation. A straightforward implementation of the time domain matrix is presented. We also compare its accuracy with well-known photoacoustic models and present reconstruction results on popular phantom images.

II. Wave equation and solution

The equation governing photoacoustic wave propagation in a homogeneous medium is given by [7]

$$\frac{\partial^2 p(\mathbf{r},t)}{\partial t^2} - c^2\nabla^2 p(\mathbf{r},t) = \Gamma\frac{\partial}{\partial t}H(\mathbf{r},t), \tag{1}$$

where $\mathbf{r}$ is the spatial location, c is the speed of sound in the medium, Γ is the Grüneisen coefficient that represents light to sound conversion efficiency. Under the assumption of stress confinement, the source term can be written in a separable form as $H(\mathbf{r},t) = h(\mathbf{r})\delta(t)$. The Green's function solution for the wave equation provides pressure at a detector location $\mathbf{r}_s$ propagated from $\mathbf{r}$ over time t is given by,

$$p(\mathbf{r}_s,t) = \frac{1}{4\pi c}\frac{\partial}{\partial t}\int_{|\mathbf{r}_s-\mathbf{r}|=ct}\frac{p_0(\mathbf{r})}{|\mathbf{r}_s-\mathbf{r}|}\delta(t), \tag{2}$$

where $p_0(\mathbf{r}) = \Gamma h(r)$ is the initial pressure distribution. In most models, the time derivative is ignored, and the velocity potential given by spherical averaging is used [8]. Implementing this matrix is highly inaccurate since the accuracy of spherical averaging mainly depends on the interpolation kernel used. In this work, we show that a simple and accurate matrix can be constructed from the solution to the initial value problem in (1) [7],

$$\left(\frac{\partial^2}{\partial t^2} - c^2\nabla^2\right)p(\mathbf{r},t) = 0, \tag{3}$$

978-1-5090-3370-6/16/$31.00 ©2016 IEEE

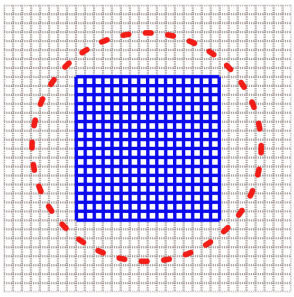

Fig. 1. Image grid (Inner), transducer location (Circular configuration) and k-space grid (Outer).

with initial conditions $p_0(\mathbf{r}) = p(\mathbf{r}, 0) = \Gamma h(\mathbf{r})$ and $\partial p/\partial t|_{t=0} = 0$. The pseudo-spectral solution to the initial value problem in Fourier space $\mathbf{k}$ at the location $\mathbf{r'}$ and time t is given by [9],

$$p(\mathbf{r'}, t) = \frac{1}{(2\pi)^3} \int \{ \int p_0(\mathbf{r}) e^{i\mathbf{k}.(\mathbf{r'}-\mathbf{r})} d\mathbf{r} \} cos(ckt) d\mathbf{k}, \quad (4)$$

where $k = |\mathbf{k}|$.

III. Pseudo-spectral matrix

The equation in (4) forms the basis for computing wave propagation at all points in a plane for a particular time instant. However, by limiting the pressure computation only to transducer locations and evaluating it over multiple time steps, we use the same equation to build the system matrix. Pseudo-spectral methods are typically implemented on a 3D grid. For simplicity and without loss of generality, a 2D grid is used in this work. The computation is performed over two grids as show in Fig. 1. The inner grid is used to define the initial pressure distribution and the outer grid is used for the k-space computation. While transducers can take any arbitrary location in the plane inside the bigger grid, we consider the commonly used circular configuration. It is important to note that pressure waves escaping from one side of the grid will re-enter on the other side due to the periodicity property of the Fourier transform. To prevent transducers from measuring the re-entered waveform, a zero padding layer is used. Let the maximum distance between any two initial pressure location occur at diagonal of imaging grid, we extend the k space, greater than half of this distance so that re-entering waves do not reach the transducers. We also ensure that the maximum time step is limited to the time taken for the farthest point in the imaging grid to reach any transducer. This limits the re-entering waves from reaching the transducer. Consider an imaging grid (inner grid) having N_{in} grid points along each axis, resulting in N_{in}^2 grid points in 2D, with co-ordinates $\mathbf{r} = (x, y) = (m * d, n * d)$. Where x and y are grid points of the 2D grid with center as origin and an equal grid spacing of d units, $(m, n) \in [-N_{in}/2, N_{in}/2 - 1]$ are integers representing index. The Fourier transform is computed on the bigger grid with frequency bins,

$$\mathbf{k} = (k_x, k_y) = \frac{2\pi}{N_{out} * d} * (u, v),$$

with N_{out}^2 grid points in a 2D grid, $(u, v) \in [-N_{out}/2, N_{out}/2 - 1]$ are integers representing index of k-space (with $N_{out} > N_{in}$). By vectorizing $\mathbf{r}$ to $\bar{\mathbf{r}}$ and $\mathbf{k}$ to $\bar{\mathbf{k}}$ we can compute the discrete Fourier transform using simple matrix multiplication as shown below.

$$\mathbf{X}_0 = \mathbf{W}_{fwd} \mathbf{x}_0, \quad (5)$$

where $\mathbf{x}_0$ is vectorized initial pressure distribution $p_0(r)$, and $\mathbf{X}_0$ is its Fourier transform. Following standard notation, $\mathbf{W}_{fwd}$ can be written as

$$\mathbf{W}_{fwd}(i, j) = \frac{1}{N_{out}} e^{-\sqrt{-1}\bar{\mathbf{k}}(i).\bar{\mathbf{r}}(j)},$$

where $\mathbf{W}_{fwd} \in \mathbb{C}^{N_{out}^2 \times N_{in}^2}$. The inverse Fourier transform is computed only at the transducer location $\bar{\mathbf{r}}_s = (x_s, y_s)$,

$$\mathbf{x}_{s_t} = \mathbf{W}_{inv} \mathbf{X}_t. \quad (6)$$

Assuming N_s transducer locations, $\mathbf{W}_{inv}$ is given by

$$\mathbf{W}_{inv}(s, i) = \frac{1}{N_{out}} e^{\sqrt{-1}\bar{\mathbf{k}}(i).\bar{\mathbf{r}}_s(s)},$$

where $s = 1, 2, \ldots, N_s$ are the transducer indices, $\mathbf{W}_{inv} \in \mathbb{C}^{N_s \times N_{out}^2}$. The wave propagation from $\mathbf{X}_0$ to $\mathbf{X}_t$ for any time instant t can be written as

$$\mathbf{X}_t = \boldsymbol{\kappa}_t \circ \mathbf{X}_0, \quad (7)$$

where $\boldsymbol{\kappa}_t = [cos\{c\bar{\mathbf{k}}(1)t\}, cos\{c\bar{\mathbf{k}}(2)t\}, \ldots, cos\{c\bar{\mathbf{k}}(N_{out}^2)t\}]^T$ and $\circ$ represents element-wise multiplication. We can now combine the matrices in (7) and (6) to measure $\mathbf{X}_0$ directly at transducer location at a time instant t.

$$\mathbf{K}_t = \mathbf{W}_{inv} \circ \left(\mathbf{1} \boldsymbol{\kappa}_t^T \right), \quad (8)$$

where $\mathbf{1}$ is a column vector of ones with a length of N_s. $\mathbf{K}_t \in \mathbb{C}^{N_s \times N_{out}^2}$ combines the propagation and Fourier inversion for a particular time instant. Stacking $\mathbf{K}_t$ for different time instants, one can construct matrix $\mathbf{K}$ which captures the response of transducers over the entire time steps. The system matrix can now be obtained by simple matrix multiplication

$$\mathbf{H} = \mathbf{K}\ \mathbf{W}_{fwd}. \quad (9)$$

Now measurements at transducer location for all time instant can be written as,

$$\mathbf{y} = \mathbf{H}\mathbf{x}_0. \quad (10)$$

It should be noted that the size of the system matrix reduces to $N_s N_t \times N_{in}^2$, and the effect of the bigger grid in the k-space has been eliminated. Although matrix formation is memory intense, it is a one-time process and a much smaller matrix is used for inversion. We first demonstrate the accuracy of the proposed matrix by comparing it with the k-wave toolbox, an open source software for photo-acoustic simulation [10]. Transducers measuring pressure time series from a point source on a 2D plane using k-wave and the proposed pseudo-spectral matrix under similar conditions, is shown in Fig. 2. It can be easily seen that the proposed approach is identical to the k-wave model. In addition to that, it can be observed

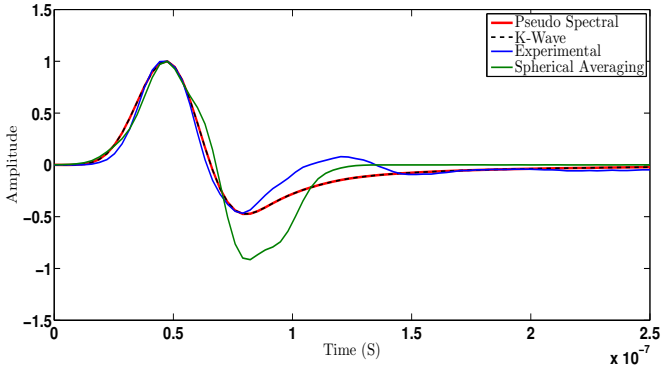

Fig. 2. Measured pressure by a single transducer propagated from a point source using pseudo-spectral matrix, k-wave toolbox and spherical averaging compared against experimental signal.

in Fig. 2 that the widely used spherical averaging model in equation (2) deviation from the expected signal. This further emphasis the accuracy and scope of the proposed matrix.

IV. Region of Interest Based Reconstruction

Once the measurements are made, the image can be recovered using matrix inversion methods. Depending on the application, the best-suited inversion process can be adopted. A straightforward approach to invert (10) is to take the l_2 norm of the residue as the cost function and minimize it for image reconstruction. In other words,

$$\hat{\mathbf{x}}_0 = \underset{\mathbf{x}}{\operatorname{argmin}} \|\mathbf{H}\mathbf{x} - \mathbf{y}\|_2^2. \tag{11}$$

If we have prior knowledge that the tomographic slice is smooth in nature we can add an additional regularization conditions such as Tikhonov regularization and formulate the optimization as

$$\hat{\mathbf{x}}_0 = \underset{\mathbf{x}}{\operatorname{argmin}} \ \|\mathbf{H}\mathbf{x} - \mathbf{y}\|_2^2 + \lambda_1 \|\mathbf{x}\|_2^2, \tag{12}$$

where λ_1 is the Tikhonov regularization constant. The additional term provides a lowpass effect, and the reconstruction is applicable for smooth objects of interest such as imaging Sentinel Lymph Nodes and dye tracking [2]. In most of the photo-acoustic studies vascular structures of human and small animals are performed [2]. These images are usually sparse in nature and can be reconstructed using a sparsity based regularization term instead of the smoothing term in (12). Sparsity can be promoted using l_1 norm and the cost function can be modified to [4], [3], [11],

$$\hat{\mathbf{x}}_0 = \underset{\mathbf{x}}{\operatorname{argmin}} \ \|\mathbf{H}\mathbf{x} - \mathbf{y}\|_2^2 + \lambda_2 \|\mathbf{x}\|_1, \tag{13}$$

where the parameter λ_2 can be either used to give priority to sparsity or to reduce the residual error. This recovery approach became very popular in photo-acoustic tomography because it can recover the image with far fewer measurements and it is known as compressed sensing. It is also applicable for non-sparse images since sparsity in a transform domain is natural. Depending on the nature of the image, a sparsifying basis like the wavelet transform or the Fourier transform can be used in the recovery. If $\mathbf{\Psi}$ is a sparsifying matrix, then $\mathbf{x}$ can be sparsely represented as

$$\boldsymbol{\theta} = \mathbf{\Psi}\mathbf{x}.$$

Then, by modifying the objective function in (13), we can recover $\boldsymbol{\theta}$. Let $\hat{\boldsymbol{\theta}}_0$ be the optimum solution

$$\hat{\boldsymbol{\theta}}_0 = \underset{\boldsymbol{\theta}}{\operatorname{argmin}} \ \|\mathbf{H}\mathbf{\Psi}^{-1}\boldsymbol{\theta} - \mathbf{y}\|_2^2 + \lambda_3 \|\boldsymbol{\theta}\|_1. \tag{14}$$

From optimal solution $\hat{\boldsymbol{\theta}}_0$, $\hat{\mathbf{x}}_0$ can be reconstructed by applying the inverse of the sparsifying basis $\mathbf{\Psi}$. In head and abdominal imaging another variant of this cost function can be used namely Total Variance (TV) minimization. This reconstruction is preferred when there are smooth regions separated by sharp edges as in the tomographic slice of a head [2]. TV minimization is known to preserve edges and can be obtained by solving the optimization

$$\hat{\mathbf{x}}_0 = \underset{\mathbf{x}}{\operatorname{argmin}} \ \|\mathbf{H}\mathbf{x} - \mathbf{y}\|_2^2 + \lambda_4 \|\mathbf{x}\|_{TV}. \tag{15}$$

V. Results and Discussion

To validate our model, the PA signal from the model is compared with experimental signal. VISULAS YAG III from Zeiss is used as the pulse laser source, which has a pulse width of $3ns$ at 1064nm wavelength. A black nylon thread of $60\mu m$ is used as an absorber. An Olympus V384 transducer is used as a detector, with the center frequency (f_c) of $3.5MHz$ and a bandwidth of 60% of f_c at $-6dB$. Both absorber and transducer are immersed in a water tank and a laser is manually triggered from outside the tank. A similar setting is used in the simulation. Fig. 3 shows that the PA signal from proposed model agrees well with the experimental signal. The second peak in the experimental PA signal is due to the PA signal generated from the wall of water tank. This can be eliminated using a careful design of the experimental setup. It can also be noted that signal from the proposed model is perfectly agreeing with signal obtained from k-wave toolbox [10] Fig. 3. The k-wave is an open source toolbox for PAT simulation. We have also compared these signals with the widely used spherical averaging model. It can be observed from the Fig. 3 that spherical averaging model deviates from the experimental PA signal. This is due to the error associated with the discretization of the model.

The main computational advantage of the proposed method over k-wave toolbox is two fold. Firstly, for the model computation the proposed model uses one forward Fourier operation and the number of inverse Fourier operations is equal to the number of time steps. While k-wave uses three coupled first order equations, resulting in a minimum of 6 and maximum of 14 fft operations at each time step [10]. In addition to that mostly in tomography, system parameters like source and detector configurations are fixed. This result in a single time computation of system matrix. Once the matrix is generated, measurements are obtained simply using matrix multiplication, which is many times faster than k-wave iterative computation

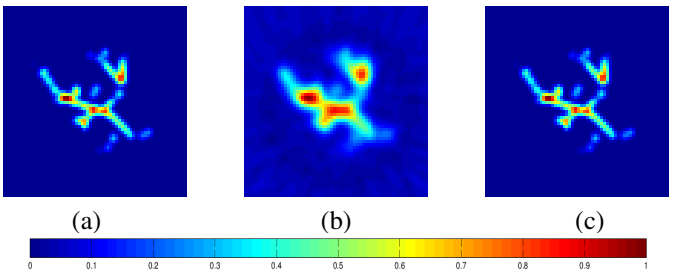

Fig. 3. (a) Original image, from measurements at Nyquist rate (b) reconstructed using k-wave (SSIM = 0.5009) (c) reconstructed using pseudo inverse of proposed matrix (SSIM = 0.9997)

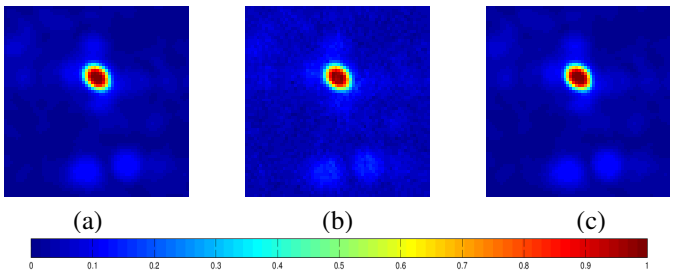

Fig. 4. (a) Original image, reconstruction using Tikhonov regularization (L-curve regularization) with (b) proposed matrix (SSIM = 0.9029) (c) with impulse response matrix (SSIM = 0.9991) [5]

using first order equations. The only problem associated with the proposed method is its memory requirement, that we overcome by utilizing the sparsity of the matrix.

Numerical simulations are performed on a 64×64 imaging grid, with a 256×256 k-space grid. Grid spacing is taken as $d = 0.1mm$ and point detectors are placed $5mm$ out side the imaging grid as shown in Fig. 1. Assuming the sound constant to be $c = 1500m/s$, the maximum frequency generated by the grid can be calculated as $c/(2{*}d) = 7.5MHz$. This calculation is based on the Nyquist sampling theorem. In our simulations, acoustic waves are measured over a time period of $5\mu s$ and the number of samples required according to the Nyquist rate is 75. In all our experiments, a circular configuration of 64 transducers was used. In the first experiment, signals are taken at Nyquist rate and reconstruction using pseudo-inverse of the matrix and using the k-wave toolbox is shown in Fig. 3. In this case, the matrix is over-determined and the pseudo-inverse gives a perfect reconstruction while time reversal using k-wave is highly inaccurate. In all the experiment quality of reconstruction is measured using the Structural SIMilarity (SSIM) index [12]. In the second experiment, imaging a Sentinel Lymph Node is considered. A sub-Nyquist sampling is performed and the number of samples are taken to be 64. Since tomographic image is expected to have a smooth nature, Tikhonov regularization is used as in (12). Fig. 4 shows the reconstruction using regularization parameters obtained from the L-curve with both proposed matrix and impulse response matrix [5]. With Tikhonov regularization impulse response matrix works slightly better than proposed matrix since it is specifically designed to work with this approach. Imaging head and abdomen of small animal requires a trade-off between preserving edges and smooth structures. We use TV minimization as in (15) to solve this problem. The reconstruction is demonstrated with the Shepp-Logan (head) phantom. This approach can reconstruct image from highly under-sampled signals with prior knowledge of the region of interest. Reconstruction from 32 and 20 samples are shown in Fig. 5. It is shown that perfect reconstruction is possible at far lower rates than the Nyquist rate. This reconstruction is widely used in compressed sensing based image reconstruction. l_1 minimization is a generic compressed sensing method which can reconstruct a large class sparse signals. If the signal is

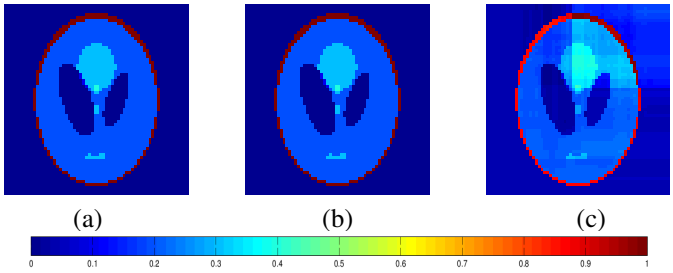

Fig. 5. (a) Original image, reconstruction using total variance minimization (b) from 32 samples (SSIM = 1) (c) from 20 samples (SSIM = 0.7421).

sparse in a basis, and if the basis is incoherent with the measurement matrix then l_1 minimization provides the best sparse reconstruction. In our experiments, a sparse vascular structure phantom is used and reconstructions from 32 and 22 randomly selected measurements are shown in Fig. 6 (a, b, c). Under similar measurement conditions we also compare reconstruction using l_1 minimization, using an impulse response matrix from [5], a spherical averaging matrix from [3] and a frequency domain matrix from [4] in Fig. 6 (d, e, f). From the comparison it is clear that reconstruction using the proposed matrix works better than all time domain matrices. The result is also comparable with frequency domain matrix which requires the entire measurements to be transformed to the frequency domain for inversion. Our proposed matrix on the other hand absorbs both the forward and inverse Fourier operations and operates directly on the time domain samples, and thereby offers higher computational efficiency.

VI. Conclusion

We presented a simple and accurate measurement matrix that models wave propagation in Photo-Acoustic Tomography. The accuracy of measurements using the matrix is validated and reconstruction based on region of interest is also demonstrated. Reconstruction using the proposed matrix is better than spherical averaging and impulse response based matrices and on par with the frequency domain matrices. These advantages make the proposed matrix attractive for model based photoacoustic imaging.

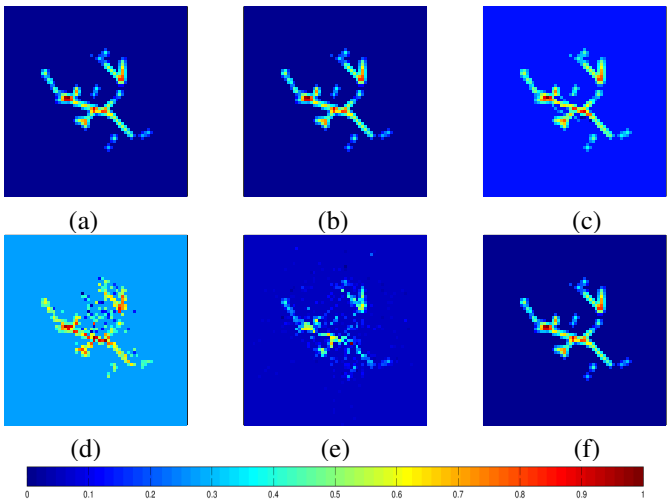

Fig. 6. (a) Original image, reconstruction using l_1 minimization with proposed matrix, (b) from 32 samples (SSIM = 1), (c) from 22 samples (SSIM = 0.9412), (d) from 22 samples using impulse response matrix [5] (SSIM = 0.7885) (e) from 22 samples using spherical averaging matrix [3] (SSIM = 0.7802) (f) from 22 samples using frequency domain matrix [4] (SSIM = 1).

REFERENCES

[1] Andrew C Tam, "Applications of photoacoustic sensing techniques," *Reviews of Modern Physics*, vol. 58, no. 2, pp. 381, 1986.

[2] Lihong V Wang and Song Hu, "Photoacoustic tomography: in vivo imaging from organelles to organs," *Science*, vol. 335, no. 6075, pp. 1458–1462, 2012.

[3] Zijian Guo, Changhui Li, Liang Song, and Lihong V Wang, "Compressed sensing in photoacoustic tomography in vivo," *Journal of Biomedical Optics*, vol. 15, no. 2, pp. 021311–021311, 2010.

[4] Jean Provost and Frederic Lesage, "The application of compressed sensing for photo-acoustic tomography," *Medical Imaging, IEEE Transactions on*, vol. 28, no. 4, pp. 585–594, 2009.

[5] Jaya Prakash, Aditi Subramani Raju, Calvin B Shaw, Manojit Pramanik, and Phaneendra K Yalavarthy, "Basis pursuit deconvolution for improving model-based reconstructed images in photoacoustic tomography," *Biomedical optics express*, vol. 5, no. 5, pp. 1363–1377, 2014.

[6] Chao Huang, Kun Wang, Liming Nie, Lihong V Wang, Mark Anastasio, et al., "Full-wave iterative image reconstruction in photoacoustic tomography with acoustically inhomogeneous media," *Medical Imaging, IEEE Transactions on*, vol. 32, no. 6, pp. 1097–1110, 2013.

[7] BT Cox and PC Beard, "Fast calculation of pulsed photoacoustic fields in fluids using k-space methods," *The Journal of the Acoustical Society of America*, vol. 117, no. 6, pp. 3616–3627, 2005.

[8] Peter Kuchment and Leonid Kunyansky, "Mathematics of thermoacoustic tomography," *European Journal of Applied Mathematics*, vol. 19, no. 02, pp. 191–224, 2008.

[9] Kun Wang and Mark A Anastasio, "A simple fourier transform-based reconstruction formula for photoacoustic computed tomography with a circular or spherical measurement geometry," *Physics in medicine and biology*, vol. 57, no. 23, pp. N493, 2012.

[10] Bradley E Treeby and Benjamin T Cox, "k-wave: Matlab toolbox for the simulation and reconstruction of photoacoustic wave fields," *Journal of biomedical optics*, vol. 15, no. 2, pp. 021314–021314, 2010.

[11] KJ Francis, P Rajalakshmi, and Sumohana S Channappayya, "Distributed compressed sensing for photo-acoustic imaging," in *Image Processing (ICIP), 2015 IEEE International Conference on*. IEEE, 2015, pp. 1513–1517.

[12] Zhou Wang, Alan Conrad Bovik, Hamid Rahim Sheikh, and Eero P Simoncelli, "Image quality assessment: from error visibility to structural similarity," *Image Processing, IEEE Transactions on*, vol. 13, no. 4, pp. 600–612, 2004.